Engineering and Technology Journal
Journal homepage: https://etj.uotechnology.edu.iq

Investigating the effect of electroplated coatings on single-phase fluid flow and heat transfer in microchannel

Hasan Q. Hussein[a*], **Ekhlas M. Fayyadh**[b], **Moayed R. Hasan**[b]

[a] Petroleum Engineering Dept., Kerbala University, Karbala 56001, Iraq.
[b] Mechanical Engineering Dept., University of Technology-Iraq, Alsina'a Street, 10066 Baghdad, Iraq.
*Corresponding author Email: 19.30@grad.uotechnology.edu.iq

HIGHLIGHTS

- An experimental study was conducted for single-phase flow in the microchannels.
- The heat transfer performance of materials coated with Al_2O_3 is enhanced for all Reynolds numbers.
- The fanning friction factor for Al_2O_3-coated microchannels is 3.65% greater than that of ordinary microchannels.
- Nusselt number of microchannel models coated with Al_2O_3 was 11.07 percentage points higher than that of the normal microchannel.

ARTICLE INFO

Handling editor: Sattar Aljabair

Keywords:
Single-phase fluid flow;Heat transfer; Microchannels;Electroplating Al_2O_3 coating; Enhanced performance.

ABSTRACT

A significant heat flux affects the efficacy and durability of most equipment. Cooling these devices is the primary concern, prompting specialists to propose and investigate various solutions. For these applications, microchannels are regarded as a possibility. Experiments were conducted in this study to determine the effect of an electroplating coating on the characteristics of a single-phase flow. As the working fluid for the experiments, deionized water was used. During the investigations, a microchannel of 0.3mm width and 0.7mm depth with an average roughness of 18.64 nm was machined; the inlet temperature was maintained at 30˚C, and the Reynolds number ranged from 109.2 to 2599. According to the results, the correlation between the fanning friction factor and laminar and turbulent flows can predict experimental findings with high precision. In addition, an increase in the Nusselt number correlates with an increase in the Reynolds number.When compared to a conventional microchannel, the models with an Al_2O_3 cladding have a fanning friction factor that is much greater. According to the results, a reliable correlation can be used to precisely estimate the friction factor of typical Al_2O_3-coated microchannels. The results demonstrated that the average value of the maximum thermal performance value was approximately 1.19 at low Reynolds numbers between 240-480 and then decreased as Reynolds numbers increased.

1. Introduction

Over the past three decades, the relentless miniaturization of electronic components has generated an urgent need for extra trustworthy thermal management solutions that dependably keep the system temperatures below certain material and performance constraints. This trend began about 1980 when an increase in heat dissipation drove a transition from the fan-cooled heat sink attachments to the liquid-based cooling methods. Initially, a liquid solution for cooling a single-phase flow was used [1].

Investigators have looked at both the movement of fluid and the transmission of heat through microchannels. It was clarified why certain outcomes depart from predictable correlations, as evidenced by entrance effects, temperature-dependent features, compression effects, combined heat transfer, surface roughness, viscosity heat, surface roughness, scaling effects, and experimental errors. In other words, it was shown that the inlet effects, temperature-dependent features, and compression effects were all responsible. It is currently unknown which factors impact the behavior of flow and heat transmission in microchannels. Numerous investigators found that heat transport in microchannels diverged from what the conventional theory and macro-scale correlations had anticipated. Harms et al. [2] experimentally investigated the single-phase forced convection of a flow of deionized water passed via both single and multi-deep rectangular silicon microchannels with a wall thickness of 119 micrometers and a width of 251 micrometers for a Reynolds number range of (193-12900) based on a microchannel hydraulic diameter. At all tested flow rates, the experimental values of the Nusselt number for a single microchannel originated to exceed expected values. Although the Nusselt number was comparable to conventional, it is only at high flow rates for applications

http://doi.org/10.30684/etj.2023.141194.1487
Received 19 June 2023; Received in revised form 29 September 2023; Accepted 03 October 2023; Available online 02 November 2023
2412-0758/University of Technology-Iraq, Baghdad, Iraq
This is an open access article under the CC BY 4.0 license http://creativecommons.org/licenses/by/4.0

involving many microchannels. Yet, the limitation on the heat exchanger size prompted the prior research into its impact on the thermo-hydraulic characteristics. Qu and Mudawar investigated the thermo-hydraulic performance of single-phase microchannel heat exchangers. The heat transfer characteristics and pressure drop for a single-phase laminar flow through a rectangular copper microchannel were determined through experimental and statistical methods. The width of the object measures 231µm, while its depth measures 713µm with a heat flux range (100 - 200 W/cm^2) explored for a Reynolds number range (139-1672) [3]. Observations and numerical predictions agreed, justifying the application of standard Navier–Stokes equations to microchannels. Despite this, several studies, such as Lee et al. [4] have investigated the Effect of hydraulic diameters on thermal performance. Lee et al. [4] analyzed the Effect of the hydraulic diameter of copper microchannels on the thermal action of a single-phase flow utilizing deionized water. They found that the microchannel width range was proportional to the hydraulic diameter (19.4534µm). Between 300 and 3500 Reynolds numbers were used for tests. It was detailed that a heat transfer coefficient rose as the channel size reduced, and the experimental results diverged significantly from conventional correlations.

Jung and Kwak [5] studied the impact of microchannel width on the friction coefficient and thermal behavior. Experimentations were done on a silicon microchannel with the same depth (100µm) and length (15mm), but the varying widths, using deionized water as the working fluid, were (100µm, 150µm, and 200µm). The relationship between heat transfer coefficient and wall temperature was declared to be linear. Moreover, the connection between the Nusselt and Reynolds numbers diverged from typical values. It was determined, however, that a friction factor through a laminar flow was equivalent to that of conventional flows. The investigation was conducted by Garcia-Hernando et al. [6], who investigated the influence of two different sizes of square stainless steel microchannels on their hydrodynamic and thermal performance. The hydraulic diameters of the microchannels were measured to be 100 µm and 200 µm. The hydraulic diameter of one of the scales was smaller than that of the other. The deionized water was employed as the working fluid. According to the conclusion, the results did not deviate from the norm. In addition, the microchannels with a minute scale did not affect the increase in heat transfer or a rise in pressure drop.

The study conducted by Mirmanto et al. [7] examined the heat transmission and fluid flow parameters in a single-phase flow within three distinct copper microchannels. These microchannels varied in hydraulic diameter (438µm, 561µm, and 635µm) and aspect ratios. The deionized water used with a mass ranging from 500 kg/m^2.s to 5,000 kg/m^2.s. It was established that the experimental friction factor and Nusselt number values for fully matured conditions were higher than the standard values. The observed variables, such as entrance effects, testing errors, pressure losses at the intake and exit, and departure from laminar flow, were considered in the experimental works. The results indicated that the standard scale water flow equations may apply to the microchannel water flows. The study conducted by Lin and Kandlikar [8] examined the influence of ordered roughness on the flow and heat transfer characteristics at the micro-scale. The evaluated roughness factors were relative roughness, roughness height, and roughness element pitch. Eight rectangular stainless steel channels of different hydraulic diameters (710-1870µm) and proximate surface roughness (0-96µm) were investigated, Utilizing water as the working fluid. The Nusselt number findings for smooth channels were appropriately predicted using a conservative correlation through developing and fully formed flow. The roughness structure was shown to raise the heat transfer coefficient. Yet, the surface with greater relative roughness had a stronger impact on the pressure drop and heat transfer. In addition, an early transition from laminar to turbulent flow occurred. In addition, it was determined that the roughness pitch of the element did not influence the heat transfer within the scope of the study.

The investigation conducted by Salem et al. [9] employed a circular microchannel made of stainless steel with a diameter of 850µm to examine the impact of surface roughness on the friction factor and heat transport. Two distinct working fluids, namely R134a and distilled water, were used, and a range of Reynolds numbers (100-10000) was considered. Despite the early identification of an early transition, the friction factor and Nu values demonstrated a stronger association with a macro-scale theory in the laminar zone. Hence, the obtained friction factor of the turbulent section may be suitably predicted by macro-scale theories. However, the observed values of the Nusselt number are less than those anticipated by correlations. According to the examination conducted by Tamayol et al. [10], the microchannel had a hydraulic diameter of 363 µm, and nitrogen was utilized as the working fluid. In this study, the utilization of an array of micro-cylinders within silicon microchannel surfaces was employed to conduct an analytical assessment of fluid flow resistance. In the experimental investigation, two methods were used: The first employed a porous medium,while the second utilized channels with varying cross-sections.

The relationship is between micro-cylinder diameter (channel size) and pressure drop. The findings demonstrated that these approaches were successful in capturing the inquiring attitude. The flexible cross-section method was extremely precise for geometric shapes in which the gap spacing ratio to the cylinder's size and the channel's height was small. However, the precision of this theory degrades as the porosity of the structure and the hole sizes significantly rise, while a porous medium strategy displayed a reasonable level of accuracy. Yet, the researchers speculated that there is a certain diameter of the micro-cylinder that should be used to minimize the pressure drop and that this diameter should be a function of the geometry of the channel and the needed surface area-to-volume ratio.

Furthermore, Xing et al. [11] studied the effect of surface roughness using three circular stainless steel microchannels with varying roughness (0.86, 0.92, and 1.02µm), nevertheless, with a similar diameter (400µm). Air with various Reynolds numbers (150-2800) was employed as a working fluid. It was determined that increasing the relative surface roughness resulted in higher Poiseuille and Nu values. In addition, when Re grew, the friction factor value dropped. In contrast, when the value of Re grew, the value of Nu increased. In addition, the transition from laminar to turbulent flow occurred at about Re = 1500, as determined by the researchers.

Markal et al. [12] studied the effect of aspect ratio through friction factor and heat transfer in microchannels with the same hydraulic diameter. In a multi-microchannel using deionized water as the working fluid, tests were conducted at a range of

Reynolds numbers (12.3-47.3). It was experimentally determined that when the aspect ratio grows, the Nusselt number increases, and the friction factor drops. In addition, the experimental Nusselt number and friction factor were found to be less than a correlation often seen. Kumar et al. [13] investigated the friction factor and Nusselt number within ten copper semi-circular multi-microchannels with a hydraulic diameter of (214μm) and a length of 60mm using deionized water as the working fluid in a single-phase flow. It was observed that a flow through a microchannel was a completely formed laminar flow and that the experimental outcomes agreed with the conventional theory of hydraulic flow. Nevertheless, with a lower Reynolds number, it was shown that the practical value of the Nusselt number departed slightly from a traditional correlation.

Huang et al. [14] examined experimentally the effect of the cavities through a single-phase pressure decrease and heat transfer. Experimentation was conducted on a 10-microchannel silicon device with a 300- μm hydraulic diameter and a 40-mm length. The experiment was performed with a low Reynolds number. Adding cavities to the microchannels improves the heat transfer and reduces the pressure drop compared to the regular microchannels. Mohammed and Fayyadh [15] conducted an experimental investigation to examine the impact of artificial cavities on the friction factor and thermal behavior of a single microchannel heat sink made of square copper with a hydraulic diameter of 300μm. The experiments used two microchannel models (model-1 and model-2) with the same hydraulic diameter. Model-1 lacked artificial cavities, whereas Model-2 featured (47) artificial cavities evenly distributed throughout the bottom surface of the microchannel. The operating fluid used was deionized water. The experimental findings manifested that the friction factor may be properly anticipated using the predictable correlation of developing flow in the laminar region for both designs. Furthermore, an experimental Nu corresponds to a laminar zone's conventional and microchannel correlations.

However, the effect of coated microchannels with silicon nanowires on the flow boiling characteristic was investigated by Alam et al., [16]. They conducted experimental studies upon the (HFE 7100) flow boiling into microchannels with plain walls and silicon nanowires (SiNW) at a range of heat and mass flux. When comparing with a bare wall, it was observed that the SiNW surface considerably reduced the flow boiling instabilities in terms of wall temperature fluctuation and pressure drop. Moreover, the SiNW performs the HTC dramatically higher than the plain wall microchannels (up to 400% improvement). On the other side, the CHF is slightly affected by nanostructured surfaces. Likewise, Wang et al. [17] investigated the Effect of etched Si nanowires upon the bottom and side walls of a parallel array of Si channels on the flow boiling characteristics using deionized water as the working fluid. Experiments were conducted at a range of heat flux and mass flux. The authors found that at a certain mass flux and heat flux state, the wall superheats degree decreased via about (15K) from (75K) to only above (60K) into the Si nano-wire-coated channels. Also, at a mass flux of (250kg/m^2.s), water's flow boiling heat transfer enhancement remained mostly unaltered while marginally increasing at higher heat fluxes. This results from the nanowires' ability to prevent the wall from drying out by capillary-assisted rewetting. For a base heat flux of around (1000 kW/m^2), a peak value of improvement (~134%) was observed at a higher mass flux (500 kg/m^2.s), but this value noticeably dropped to only (105%) as approaching the critical limit of heat flux. It was believed that the contamination-related surface wettability degradation of the coated surface through the experimentations was the reason for the lesser enhancement impact at the higher mass flux condition.

The impact of coating thermal conductivity on the overall performance is crucial to keep in mind when contemplating using coatings to improve performance. High thermal conductivity coatings can increase efficiency, whereas Gupta and Misra [18] fabricated more thermally conductive Cu-TiO_2 nanocomposite coatings on the mini channel copper heating surfaces. The experiments were performed at subcooled conditions within a heat and mass flux range, utilizing DI water as a working fluid. Results displayed that the peak enhancement by CHF (143%) and HTC (153%) was attained on a developed coated surface at lower mass flux. Bulut [19] study employed passive heat transfer improvement methods, including nanostructures and microporous sintered surfaces over open microchannel surfaces and pin-finned microchannels. This study examined microchannel impacts on seven structures in pool boiling. The microchannel with single pin-fins had the greatest HTC of 181.03 kW/(m^2 °C) at 172.61 W/cm^2. The HTC improvement was 2.8 times the ordinary surface. HTC and CHF improved on all treated surfaces relative to the copper chip baseline tested. The microchannel with single pin-fins had the greatest HTC of 181.03 kW/(m^2 °C) at 172.61 W/cm^2. The HTC improvement was 2.8 times the ordinary surface. HTC and CHF improved on all treated surfaces relative to the copper chip baseline tested.

According to the findings of the experiments, the experimental friction factor may be properly predicted for two models by utilizing a traditional correlation of developing flow in a laminar zone. This is the case for both of the models. In the laminar site, the experimental Nusselt number has a high degree of unity with conventional and microchannel correlations.

In heat transfer in microchannels with a single-phase flow, some of the research problems that must be addressed include:

- Heat transfer enhancement:

Microchannels are used in many applications where efficient heat transfer is critical, such as microprocessors, power electronics, and chemical reactors. One of the biggest challenges in microchannel heat transfer is achieving high heat transfer rates in a compact space. To address this problem, researchers are exploring ways to increase the heat transfer coefficient, such as using coatings, surface modifications, and other techniques.

- Pressure drop:

Due to the smaller cross-sectional area, the fluid flow resistance is higher in microchannels than in conventional channels. This can lead to higher pressure drops, limiting the maximum flow rate and reducing the overall heat transfer efficiency. Researchers are looking for ways to reduce the pressure drop in microchannels, such as optimizing the channel geometry, using flow modifiers, and implementing other flow control techniques.

- Thermal management:

Microchannels are commonly used for the thermal management of electronic devices, where the goal is to remove the heat from the device and dissipate it into the surrounding environment. One of the challenges in thermal management is maintaining a uniform temperature distribution across the device surface, which can be difficult in microchannels due to the complex flow patterns and heat transfer mechanisms. Researchers are exploring ways to optimize the microchannel design and flow conditions for more efficient and uniform thermal management.

- Scaling:

Microchannels, such as heat exchangers or chemical reactors, are often used in applications requiring many channels. One of the challenges in scaling up the microchannel systems is maintaining the same heat transfer efficiency and flow characteristics as in the individual channels. Researchers are investigating ways to scale up the microchannel systems while preserving their performance characteristics, such as using parallel tracks or optimizing the inlet and outlet configurations.

Overall, the research problem in heat transfer in microchannels with a single-phase flow is to optimize the heat transfer performance and the fluid flow characteristics of these systems while accounting for the unique challenges and constraints of micro-scale geometries.

This study employs an improvement method for the heat transfer performance in a single microchannel. Therefore, this study aims to investigate the coating effect on the flow and heat transfer characteristics. In addition, the friction factor and Nusselt number predicted by the model will be compared with experimental data, conventional correlations, and micro-scale correlations.

2. Experimental instruments and data reduction methodology

2.1 Setup of experiment

An experimental rig was designed and manufactured, and the system includes a deionized water tank, a micro gear pump, a preheater, a test section, a sub-cooler, and an in-line filter. Three different fields of rotameter were used as follows: Rotameter model (LZB3WBF) with a lower range (1.6-16 ml/min), a medium range (2.5-25 ml/min) of rotameter model (CX-GRM-LZB-4WB), and a higher capacity (16-160ml/min) of rotameter model (LZB4WB). The working pressure of the rotameter was 1.0325 bars. For cooling purposes, a sub-cooler and condensing unit were used. Plates 1 and Figure 1 display the experimental system setup and the schematic diagram. An intense boiling for about one hour was employed to ensure the degassing of the deionized water accumulated in the liquid tank. The non-condensable gases are relieved from the environment through an open valve at the top of the condenser. The deionized water passes through a 5µm filter installed before the gear pump to eliminate all particles from the water. Following that, the degassed water was pumped to the test section. A preheater was used to control the inlet temperature of the working fluid.

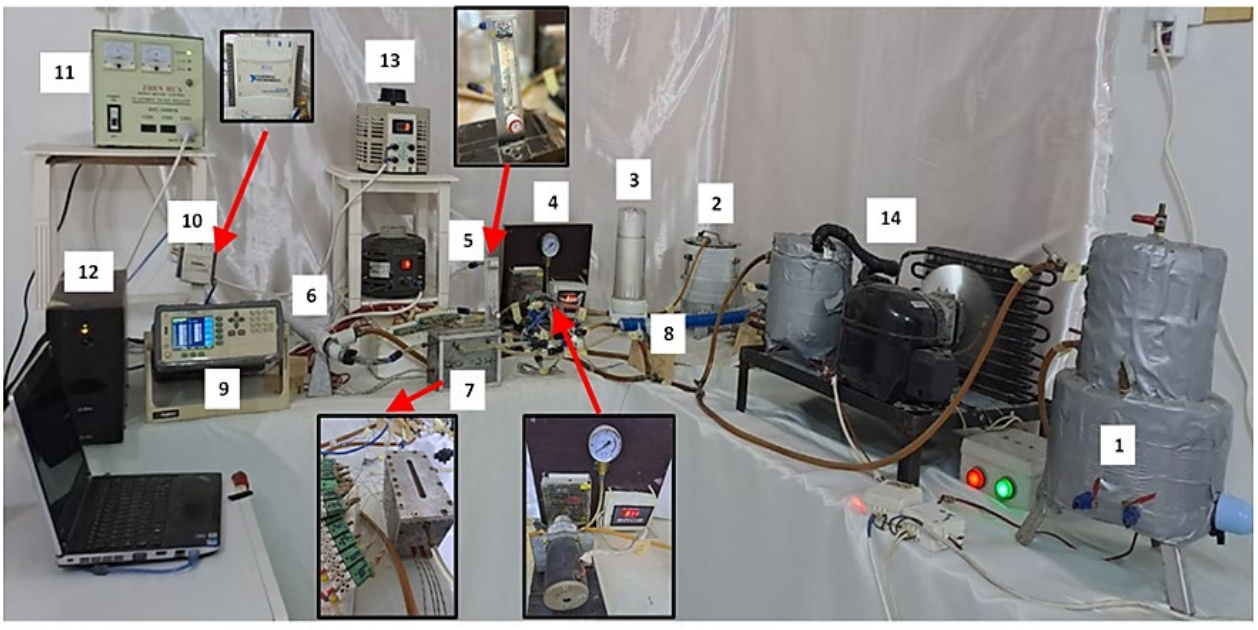

1: Degasses 2: Main Tank 3: Filter 4: Micro-Gear Pump with Controller 5: Flow meter 6: Preheater 7: Test-Section 8: Sub-Cooler

9: Data Logger 10: DAQNI6009 11: AC-Stabilizer 12: Unit Power Supply 13: Variac 14: Chiller Unit

Plate 1: The experimental facility

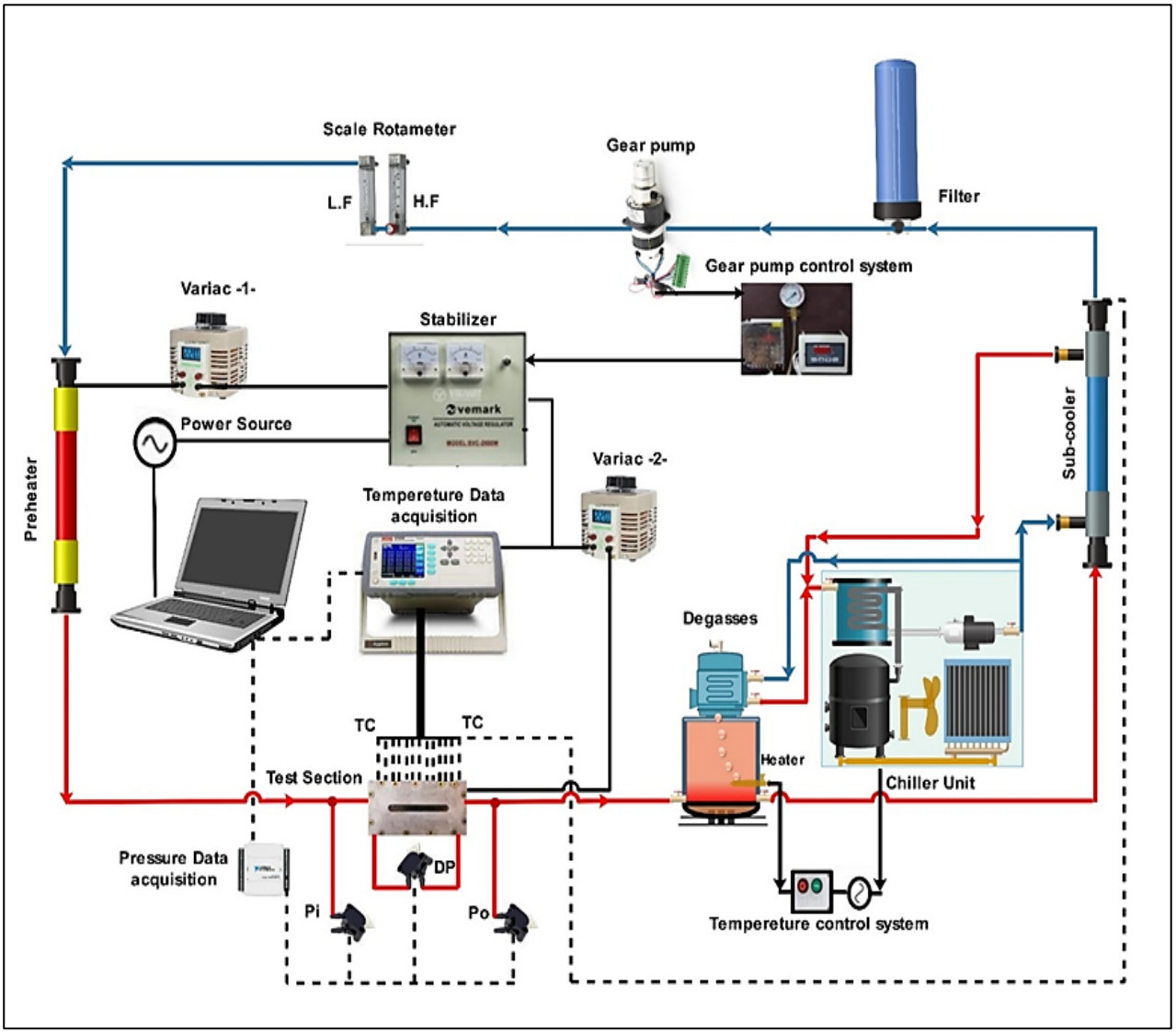

Figure 1: Schematic diagram of the experimental facility

The test section consists of brass-black (68.28 % Cu and 31.77 % Zn by weight) with a single microchannel, stainless steel housing, cartridge heaters, and a top cover plate. On the upper surface of the brass block, a single rectangular microchannel was grooved by a milling machine with a feeding rate of (10mm/min). The brass block had dimensions of (30mm width, 114mm length, and 81mm height. The microchannel was machined with 0.3mm width and 0.7 mm depth. An electronic microscope (SEM) was used to measure the width and depth of the microchannel. Two cartridge heaters of 100 W were inserted horizontally at the bottom of the brass block to supply the required heat. Four thermocouples Type K were distributed vertically along the center line of the brass block at equal distances (14.7mm) to measure the wall temperature. At 1mm from the lower surface of the microchannel, seven thermocouples of type K were axially distributed at nearly 10mm from each other. The diameter of all used thermocouples was 0.5mm, with an accuracy calibration of ± 0.5 k. The brass block was assembled with a stainless steel housing and sealed with an O-ring, as revealed in Figure 2, while Figure 3 shows the actual dimensions of the microchannel. An atomic force microscope (AFM) was used to obtain the roughness of the bottom surface of the microchannel. The microscope probe scanned over an area of 100000 x 100 000nm and evaluated an average roughness of 18.64 nm, as depicted in Figure 4. The stainless steel housing contains inlet and outlet manifolds in addition to subchannels. Two thermocouples, Type K, were immersed into subchannels to measure the temperature of the working fluid at the inlet and outlet. Two transducer types (MPX5500DP) were used to calculate the inlet and outlet pressure out of the manifold, while the pressure drop across the test section was measured using the differential pressure transducer type (MPX4250DP). The accuracy of all transducers was ± (3.21, 4.32, and 4.33%), respectively. The dimensions of the inlet and outlet manifolds were (20 x 20 x 0.7mm), while the dimensions of the inlet and outlet subchannels were (7 x 2 x 0.7mm). The top covered plate was equipped with a visualization window of the same microchannel dimensions to observe the flow through the microchannel, including subchannels. The obtained temperature data was recorded using data Logger (Applent AT 4532x) reading. The pressure transducer signals (0-5 DC–Volt)) from the pressure transducer gauge to LabView software were collected using Bus-power multifunction DAQUSB (model NI USB-6009)) as an interface device.

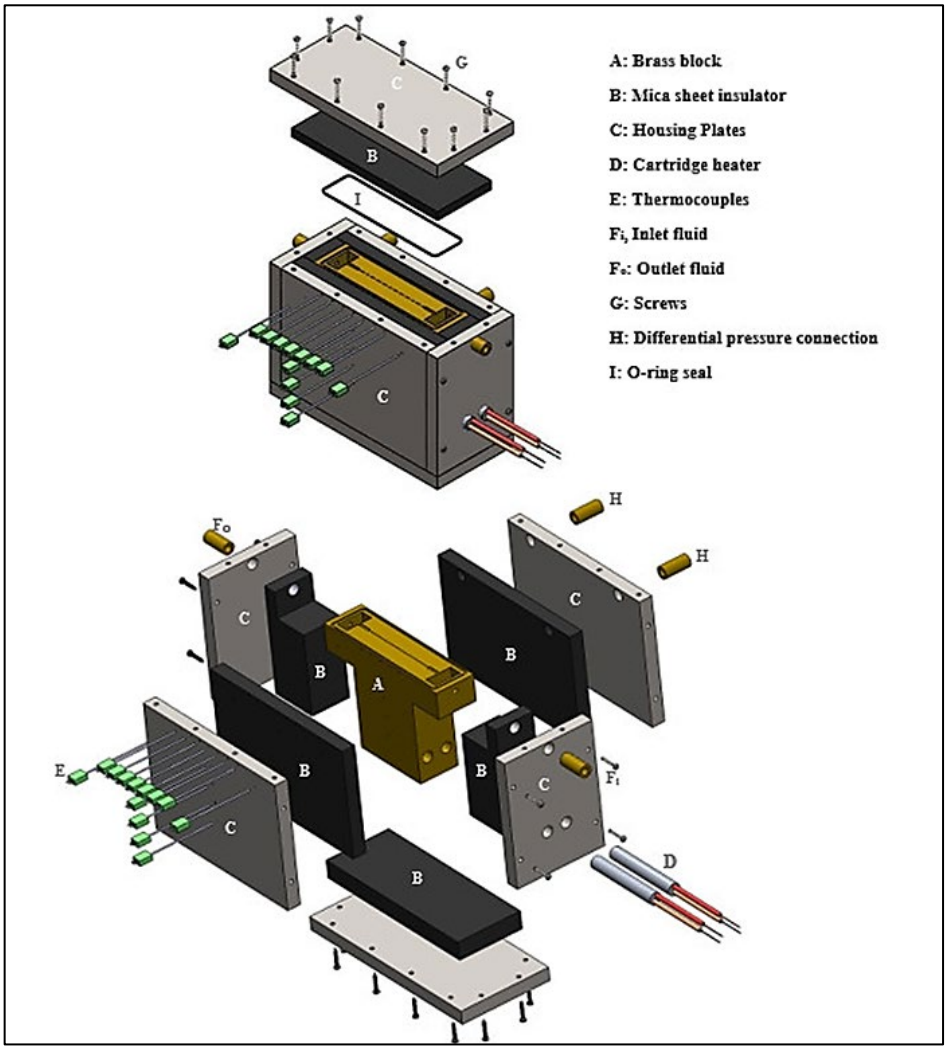

Figure 2: Schematic of the test section

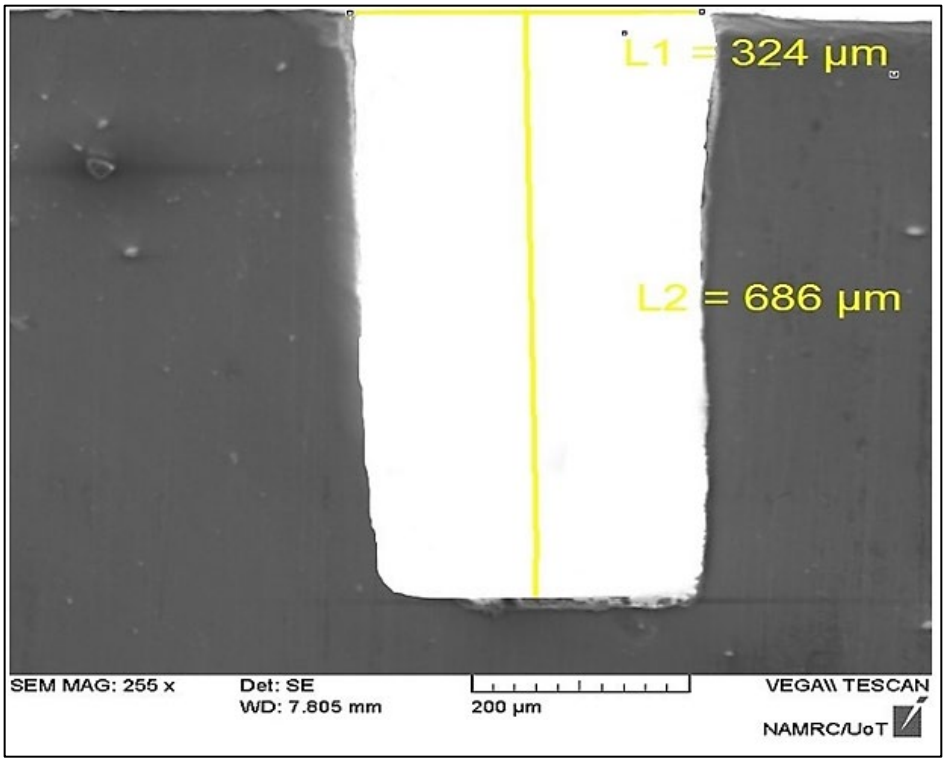

Figure 3: Microchannel actual dimensions

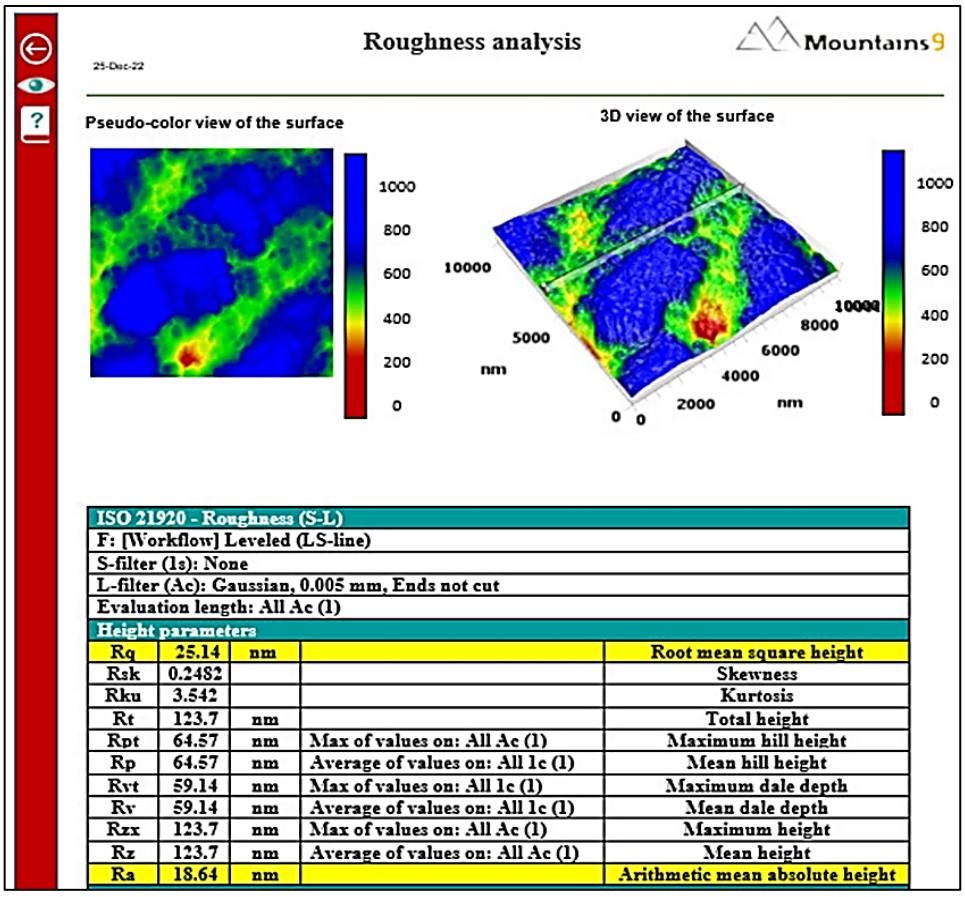

ISO 21920 - Roughness (S-L)				
F: [Workflow] Leveled (LS-line)				
S-filter (1s): None				
L-filter (Ac): Gaussian, 0.005 mm, Ends not cut				
Evaluation length: All Ac (1)				
Height parameters				
Rq	25.14	nm		Root mean square height
Rsk	0.2482			Skewness
Rku	3.542			Kurtosis
Rt	123.7	nm		Total height
Rpt	64.57	nm	Max of values on: All Ac (1)	Maximum hill height
Rp	64.57	nm	Average of values on: All 1c (1)	Mean hill height
Rvt	59.14	nm	Max of values on: All 1c (1)	Maximum dale depth
Rv	59.14	nm	Average of values on: All 1c (1)	Mean dale depth
Rzx	123.7	nm	Max of values on: All Ac (1)	Maximum height
Rz	123.7	nm	Average of values on: All Ac (1)	Mean height
Ra	18.64	nm		Arithmetic mean absolute height

(A)

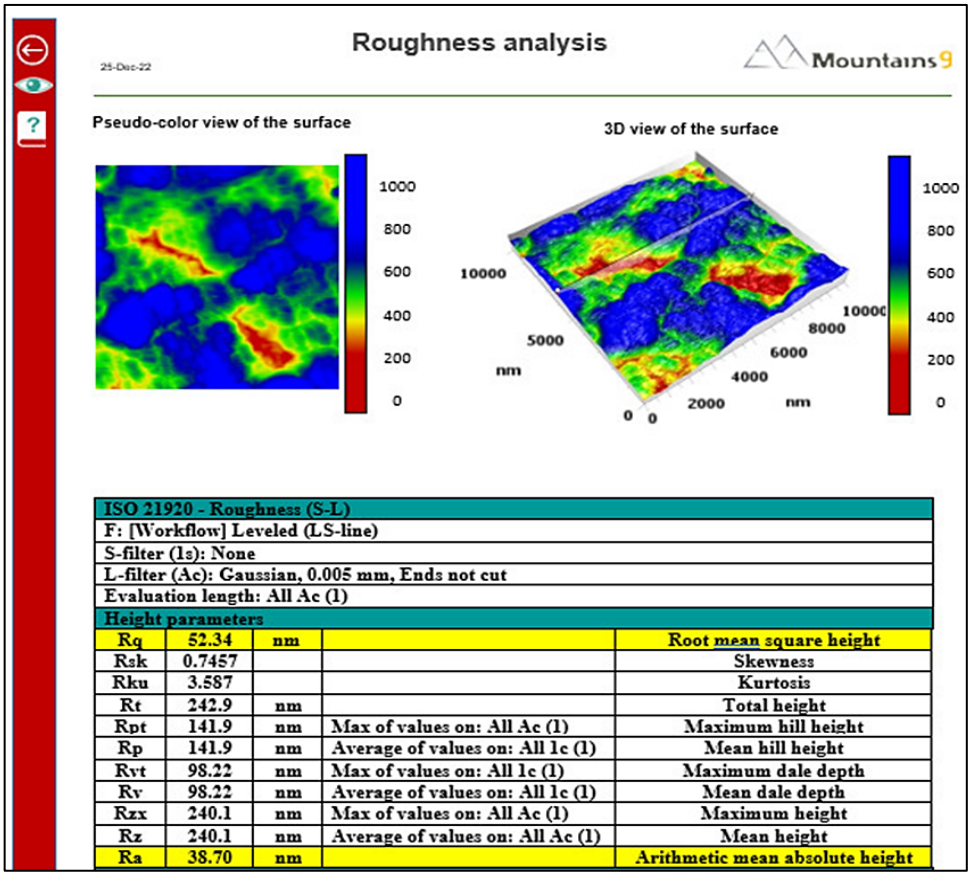

ISO 21920 - Roughness (S-L)				
F: [Workflow] Leveled (LS-line)				
S-filter (1s): None				
L-filter (Ac): Gaussian, 0.005 mm, Ends not cut				
Evaluation length: All Ac (1)				
Height parameters				
Rq	52.34	nm		Root mean square height
Rsk	0.7457			Skewness
Rku	3.587			Kurtosis
Rt	242.9	nm		Total height
Rpt	141.9	nm	Max of values on: All Ac (1)	Maximum hill height
Rp	141.9	nm	Average of values on: All 1c (1)	Mean hill height
Rvt	98.22	nm	Max of values on: All 1c (1)	Maximum dale depth
Rv	98.22	nm	Average of values on: All 1c (1)	Mean dale depth
Rzx	240.1	nm	Max of values on: All Ac (1)	Maximum height
Rz	240.1	nm	Average of values on: All Ac (1)	Mean height
Ra	38.70	nm		Arithmetic mean absolute height

(B)

Figure 4: Analysis of bottom's surface roughness for the test specimens (10000nmx10000nm) for (A) Palin and (B) coated with Al_2O_3

2.2 Electroplating method system

In this study, a single rectangular microchannel can be specified as a plain (ordinary) microchannel and a manipulated microchannel (coated with alumina). The electroplating method was used to obtain the manipulated microchannel. The electroplating system consists of a magnetic hot stirrer device, glass beaker, DC power supply, and electrolyte solution (nickel sulfate, nickel chloride, and boric acid) with specified properties, as shown in Table 1 . Figure 5 illustrates this system. Before starting the coating process, the paint sample must be polished and cleaned with ethanol alcohol. The model was immersed in a container of hydrogen chloric acid diluted in a ratio of 1:5 to remove the oxide particles adhered to the surface. Finally, the sample was placed in a container of distilled water to wash it. The electrolyte solution was put in the container and mixed quickly with the nanoparticles. Al_2O_3 (500rpm) for an hour at 50°C to get a better homogeneity of the mixture. The coating process was conducted by connecting the sample to be coated to the negative cathode, and the nickel electrode was connected to the anode and an electric current from the power supply with a value of (2.38 Amp) and (5 volts) for a period of (0.5min).

Table 1: Composition of nickel (electrolyte) bath for Al_2O_3 nanocomposite coating

Nickel sulfate ($NiSO_4.6H_2$)	Nickel chloride ($NiCl_2.6H_2O$)	Boric acid	Al_2O_3
300 g/l	45 g/l	30 g/l	Five g/l

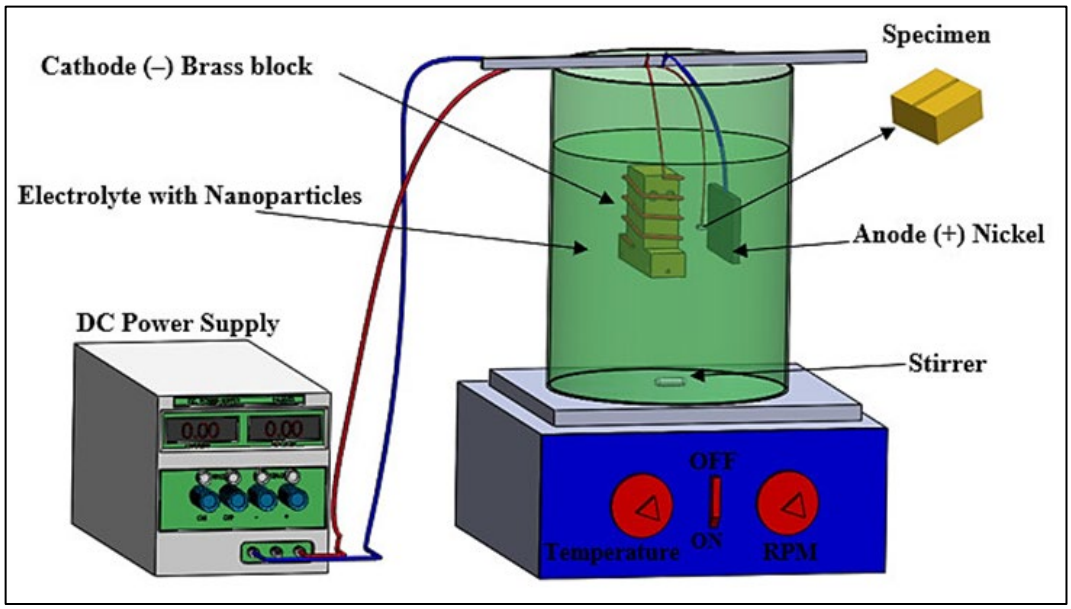

Figure 5: Schematic of electrochemical nickel plating method

2.3 Uncertainty analysis

The measurement error is the difference between the measured value and the measured quantity's real value; this difference may originate from various sources and reflects both the mistake of bias (systematic error) and random error. The bias error is brought on by the inaccuracy in the measuring equipment, and the device's calibration may bring this error down to a more acceptable level. The error brought on by external factors is the precision error (random error) (surrounding temperature, pressure, humidity, etc.). The uncertainty in each measured quantity is summarized in Table 2.

Table 2: Uncertainty value in each measured parameter

Parameter	Uncertainty
Hydraulic diameter, Dh[mm]	$\pm 2.36\%$
Heat transfer area A_{ht}[mm]	$\pm 2.2\%$
Mass flux, G [kg/m^{2}s]	$\pm 8.2 - 13.07\%$
Channel Fanning friction factor, f_{ch}	$\pm 0.5 - 4.94\%$
Wall heat flux, q'_w[kW/m^2]	$\pm 0.4 - 0.44\%$
Average heat transfer coefficient, h_{sp}[kW/m^{2}K]	$\pm 10 - 14.3\%$
Average Nusselt number, Nu	$\pm 5.3 - 15.08\%$

2.4 Data analysis

In the single-phase flow through a microchannel undergoes a net pressure drop, denoted by ΔP_{ch} in Equation (1), which may be represented as [20]:

$$\Delta P_{ch} = \Delta P_m - \Delta P_{loss} \quad (1)$$

In which ΔP_m Is the measure of the pressure drop between the input and output manifold and ΔP_{loss}. That is a drop pressure caused by total minor losses, including the input subchannel. $\Delta P_{sch,i}$, the output subchannel $P_{sch,o}$, the sudden contraction ΔP_{sc} and the sudden expansion ΔP_{se} denoted in Equation (2). Therefore, it may be worked out as follows [20]:

$$\Delta P_{loss} = \Delta P_{sch,i} + \Delta P_{sch,o} + \Delta P_{sc} + \Delta P_{se} \quad (2)$$

The pressure drop that occurred as a result of total small losses was computed as a result of the rapid contraction and expansion using the Equation (3) that is shown below[21]:

$$\Delta P_{loss} = (K_{sc1} + K_{se2}).\frac{V_{sch}^2 \cdot \rho}{2} + (K_{sc2} + K_{se1}).\frac{V_{ch}^2 \cdot \rho}{2} \quad (3)$$

In the equation presented above, (Ksc1 and Ksc2) are the loss coefficients caused by the quick contraction that occurs from a manifold to a subchannel and then from a sub-channel to a micro-channel, correspondingly. In contrast, (Kse1 and Kse2) indicate loss coefficients produced by a rapid expansion from microchannels to a subchannel and from subchannels to manifolds, respectively. The values for loss coefficients (Ksc1, Ksc2, Kse1, and Kse2) are 0.5, 0.47, 0.72, and 0.81[18]. So, Equation (4) may be used to calculate experimentation's fanning friction factor based on micro-channel pressure drop [20]:

$$f_{ch} = \frac{\Delta p_{ch} D_h}{2L\rho V_{ch}} \quad (4)$$

The Equation (5) was used to compute the base heat flux ($\grave{q_b}$) at the heat sink [20]:

$$q_b^{"} = \frac{P - Q_{loss}}{A_b} \quad (5)$$

$$P = IV \quad (6)$$

wherever in Equation (6) P represents the power of heating in watts, (I) and (V) are electric current and voltages in ampere units and Volts units, respective, and A_b Represent the base area for the heat sink, which is computed using the base heating width (W_b) and heating length (L_{ch}) for the base plate and is provided in Equation (7) as:

$$A_b = W.L_{ch} \quad (7)$$

By heating the test section without pumping liquid, one may estimate heat loss (Q_{loss}) from the test section to the surrounding environment. After the system is stable, the power and temperature of the microchannel's bottom wall are measured and recorded. The preceding steps are repeated to calculate different electrical power levels. The equation for heat loss may be found by graphing the amount of applied electrical power against the difference in temperature between the bottom wall and the ambient temperature; several authors used this strategy. A large number of researchers have adopted this strategy [22,23].

The coefficients of local heat transfer (h_{sp} (z)) are found as Equation (8) follows:

$$h_{sp}(z) = \frac{q_b^{"} W}{(T_W(z) - T_f(z))(W_{ch} + 2H_{ch})} \quad (8)$$

H_{ch}, and W_{ch} are, respectively, the height and width of the channel. It was decided to insert local thermocouples at one millimeter's distance (th) from the base of microchannels. The thermocouple temperature data (Ttc(z)) were recalculated utilizing a one-dimension heat conduction formulation to determine the temperature of the microchannel's internal surfaces (Tw(z)), as illustrated in Equation (9) [20]:

$$T_W(z) = T_{tc}(z) - \frac{q_b^{"} th}{K_s} \quad (9)$$

The localized fluid temperature ($T_f(z)$) can be computed using the Equation (10), assuming a uniform boundary condition [24] :

$$T_f(z) = T_i + \frac{q_b^{"} W.z}{\dot{m} C_p} \quad (10)$$

The variables ($T_i, z, \dot{m}$ and C_p) represent the intake fluid's temperature, the channel's axial length, the mass flow rate, and the fluid's specific heat.

The average Nusselt number is found as Equatin (11) follows [20]:

$$Nu = \frac{1}{L_{ch}} \int_0^{L_{ch}} \frac{h_{sp}(z).D_h}{K_l} dz \tag{11}$$

Experimental data were carried out at a system pressure of 1 atm, heat flux of 60.225 kW/m^2, and range of Reynolds number (109.2-2599) utilizing deionized water as the working fluid. The range for the present experiment parameter is offered in Table 3.

Table 3: The Range of Parameters for the Present Experiment Works is Summarized Below

Models of Microchannel	Inlet temperature [^{o}C]	Reynolds number	Heat flux [kW/m^2]
Model−1: Plain Microchannel Model−2: Coatin Microchannel with Al_2O_3 (5g)	30	(109.2-2599)	60.225

3. Result and discussion

3.1 Single-phase friction factor

The investigational outcomes of the fanning friction factor model were compared with the correlation of Shah and London (1978) of developing and developing flow in a laminar flow zone. Therefore, the apparent friction factor f_{app} Developing flow at the laminar region was intended using the correlation of Shah and London denoted in Equations (12 and 13) by the following [25]:

$$f_{app} = \frac{3.44}{Re(L^*)^{1/2}} + \frac{(f_{FD}Re)+\frac{K(\infty)}{4L^*}-\frac{3.44}{(L^*)^{1/2}}}{Re(1+C(L^*)^{-0.2})} \tag{12}$$

$$L^* = L_{sp}/ReD_h \tag{13}$$

In which both $(K(\infty))$ and (C) are constant; it depends on the aspect ratio of a current study, and values are (1.7784x10-4) and (1.1962). Likewise, the Poiseuille number (fFDRe) of fully developed single-phase fluid flow was expressed in Equations (14 and 15) by Shah and London [25]:

$$(f_{FD}Re) = 24(1 - 1.35534\beta + 1.9467\beta^2 - 1.7012\beta^3 + 0.9653\beta^4 - 0.2537\beta^5) \tag{14}$$

$$\beta = \frac{w_{ch}}{H_{ch}} \tag{15}$$

Moreover, Phillis and Blasius' correlations for developing and developed flow in turbulent regions were examined. For fully developed turbulent flow, the Blasius Correlation of the Fanning friction factor is as Equation (16) follows [26]:

$$f = 0.079Re^{-0.25} \tag{16}$$

Phillips, 1987, also established the fanning friction factor denoted in Equation (17) for creating turbulent flow [26]:

$$f_{appturb.} = \left(0.0929 + \frac{1.0161D_h}{L}\right) Re^{*\left(-0.268-\frac{0.3193D_h}{L}\right)} \tag{17}$$

where Re^* It is equivalent to the Reynolds number denoted in Equation (18), which is determinable as:

$$Re^* = Re\left(2/3 + \frac{11}{24}\beta(2-\beta)\right) \tag{18}$$

The experimentally Fanning friction factor against Reynolds number of the conventional and coating microchannel as indicated in figures 6 and 7. The comparison with findings of different kinds demonstrates a correlation for laminar developed flow; Shah and London [25] came up with a prediction that had a mean absolute error (MAE) denoted in Equation (19) of 11.61% and 13.59% for the conventional and conventional Al_2O_3 coated, respectively.

$$MAE = \frac{1}{N}\sum_{j=1}^{N}\frac{|f_{pred,j}-f_{exp,j}|}{f_{exp,j}}x100\% \quad (19)$$

Meanwhile, in laminar developing flow, the correlation of Shah and London [25] offered an agreeable agreement with a mean absolute error (MAE) of 8.39% and 8.48%, respectively, for conventional, Al_2O_3 coated. In addition, they found that the data supported the correlation. On the other hand, The experiment findings for two models at a turbulent zone in fully matured were anticipated by the correlations by Blasius [29], with a mean absolute error (MAE) around 4.58% and 7.01%, respectively, for conventional and Al_2O_3 coated models. This was the case for conventional models. During the period in which turbulent developing flow was present, the correlation study conducted by Phillips [26] indicated accurate estimation with the mean absolute error (MAE) for 4.6% and 2.82% for the conventional and Al_2O_3coated, respectively. As we can see in figure 8, the effect of coating microchannels on the fanning friction factor.

In general, these results suggest that a conventional theory can accurately foresee single-phase flow friction factors in the models for micro-channels that were used and under the conditions used in the experiments. The image demonstrates that when the Reynolds number increases in the laminar area for all models, there has been a modest transition from a fully formed flow theory to a developing flow theory in the friction factor data. As a consequence of this, the length of the hydrodynamic developing flow was determined by the use of Equation (20), which was developed by Shah and Bhatti [28] for a circular tube in the laminar area as in Equation (20) follows:

$$L_{hy} = 0.056\, R_e\, D_h \quad (20)$$

Because the hydraulic diameter is comparable across all models of the microchannel, one may deduce that the hydrodynamically growing lengths will also be equivalent across all models when the Reynolds number is held constant. Figure 9 illustrates the influence of the Reynolds number on the sizes that evolve hydrodynamically for all the different types of microchannels. It is possible to conclude from a figure that the flow is plainly influenced by hydrodynamically evolving flow even at low Reynolds numbers. This conclusion may be drawn from the flow diagram.

3.2 Single-phase heat transfer

Figures 10, 11, and 12 depict the relation between the average Nusselt number and the Reynolds number of conventional and coating microchannel, respectively, at the laminar flow regime for a variety of Reynolds numbers (109.2-2599). According to these results, the values of the average Nusselt number rise with an increase Reynolds number for both conventional microchannels and coated microchannels. This behavior presents the developing heat transfer theory. The fact that the relaxing segment was not implemented into the testing section of this study is the factor that is most likely responsible for this tendency. Hence, it would appear that the flow is growing thermally. So, the term "augmentation for heat transmission" denotes the existence of a thin thermal boundary layer in a thermally developing region, which, compared to a thermally completely developed area, can potentially increase heat transfer. The length for the thermally growing entry may be determined with the use of an equation developed by Shah and London in [25], which is written as follows:

$$L_{th} = 0.056\, Re\, Pr\, D_h \quad (21)$$

According to Equation 21, as demonstrated in Figure 13, thermal entry length grows with rising Reynolds numbers and can occupy the whole channel length at Reynolds numbers near 510, as shown in Figure 13.

However, the figures also display a comparison of experimental average Nusselt numbers for conventional and coating microchannels, respectively, in the laminar regions with the correlations of Shah and London [25], which are given in Equations (22 and 23) as:

$$Nu = 8.235(1 - 10.6044\,\beta + 61.1755\ \beta^2 - 155.1803\,\beta^3 + 176.9203\beta^4 - 72.9236\,\beta^5) \quad (22)$$

$$Nu = 0.775\, L^{*(-1/3)}_{t}(fRe)^{(1/3)}_{FD} \quad (23)$$

where L^* Is a length of the channel that is dimensionless and may be expressed by an Equation (24) [27]:

$$L^*_t = \frac{L}{Re\, Pr\, D_h} \quad (24)$$

In addition, considering the correlation of Mirmanto [7] for micro-channels in the laminar zone for the developing flow denoted in Equation (25), the following seems to be:

$$Nu = Re^{0.283} Pr^{-0.513} L^{*-0.309}_{t} \quad (25)$$

The thermal performance factor can be calculated in Equation (26) as :

$$\eta = \frac{\left(\frac{Nu_{coating}}{Nu_{plain}}\right)}{\left(\frac{f_{coating}}{f_{plain}}\right)^{\frac{1}{3}}} \quad (26)$$

Nevertheless, the comparison of Shah and London [25] Correlations of developing flow with outcomes of conventional showed poor performance prediction using an MAE of 22.23%. However, a good agreeable was attained, Al_2O_3 coated, Al_2O_3 an MAE of 10.73%. While the Mirmanto correlation [7] showed poor performance prediction using an MAE of 59.47% and 43.95% for the conventional, Al_2O_3 coated, correspondingly. This may be attributed to the poor heat conductivity of all brass-surfaced models, as the correlation did not account for the material Impact. In conclusion, the experimental findings of single-phase flow demonstrate that a calibration and measuring system can provide correct outcomes for trials involving two-phase flow. Figure 14 shows the Effect of the Reynolds number on the thermal Performance Factor of conventional and coated Microchannel. Results demonstrated that the presence of Al_2O_3 coating increases heat transmission and causes growth in surface area, fluid mixing, and recirculation.

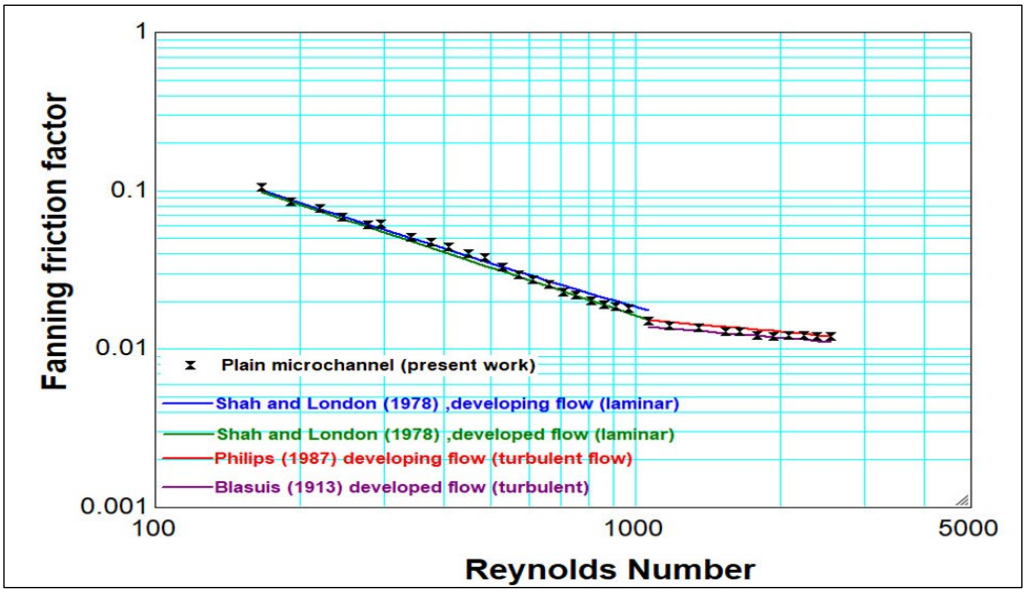

Figure 6: Experimental outcomes comparing fanning friction factor through laminar and turbulent flow correlations in plain micro-channels

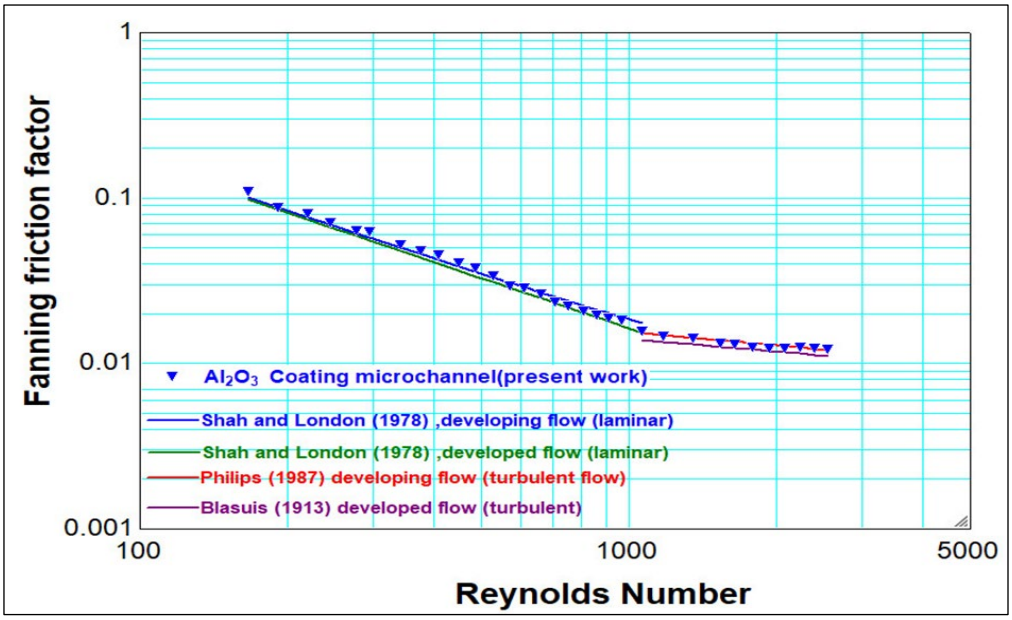

Figure 7: Experimental outcomes comparing fanning friction factor through laminar and turbulent flow correlations in the coating microchannels

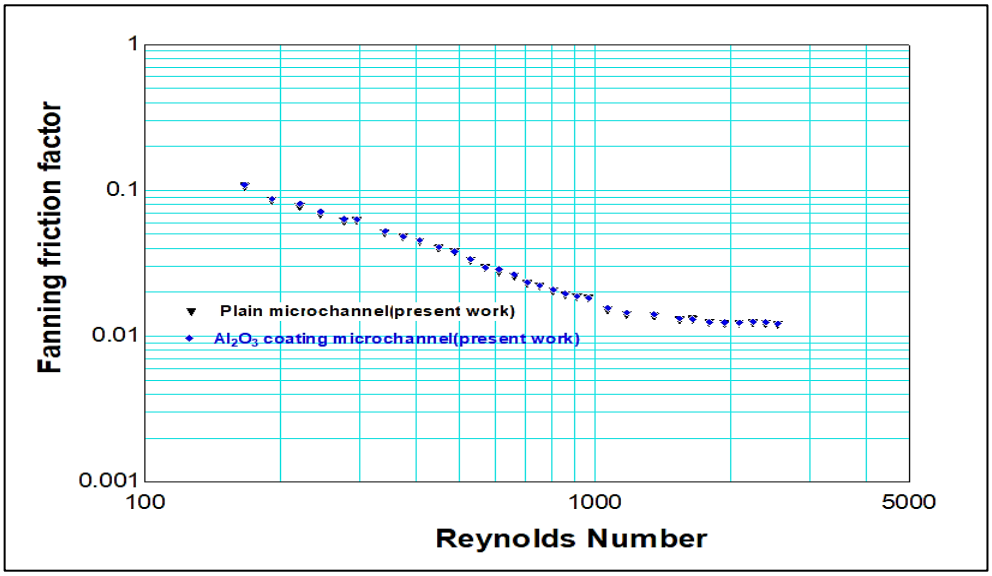

Figure 8: Effect of coating microchannel on fanning friction factor

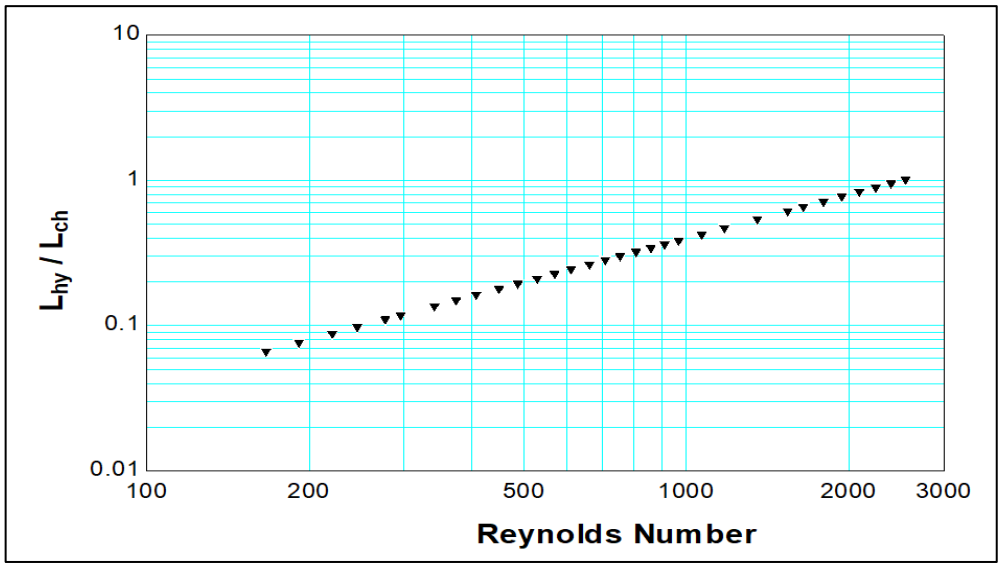

Figure 9: The influence of Reynolds number on the hydrodynamically developing micro-channel entry length

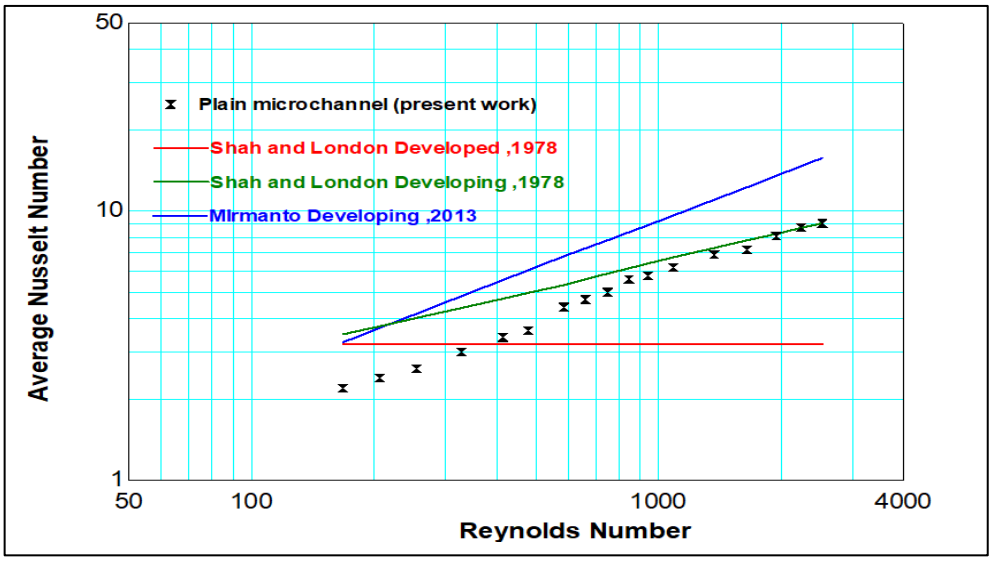

Figure 10: Comparing the experimental average Nusselt number with laminar flow correlations for plain micro-channels

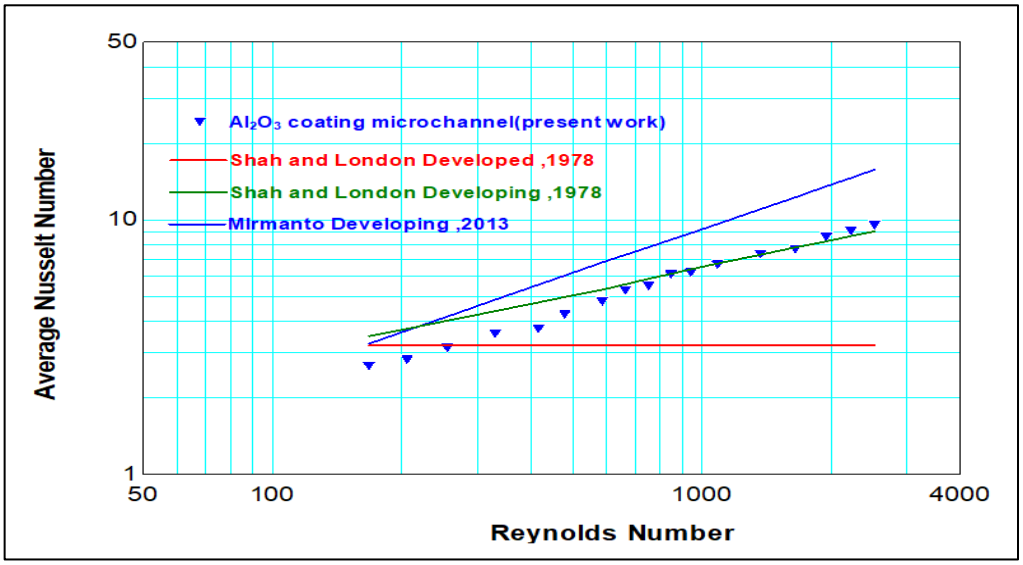

Figure 11: Comparing the experimental average Nusselt number with laminar flow correlations for coating micro-channels

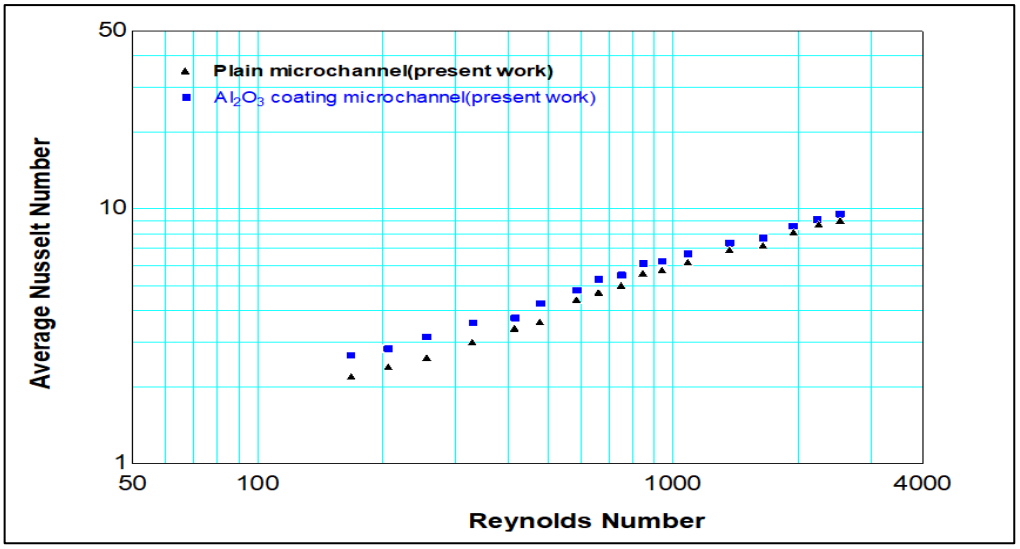

Figure 12: Comparing the experimental average Nusselt number with laminar flow correlations for coating micro-channels

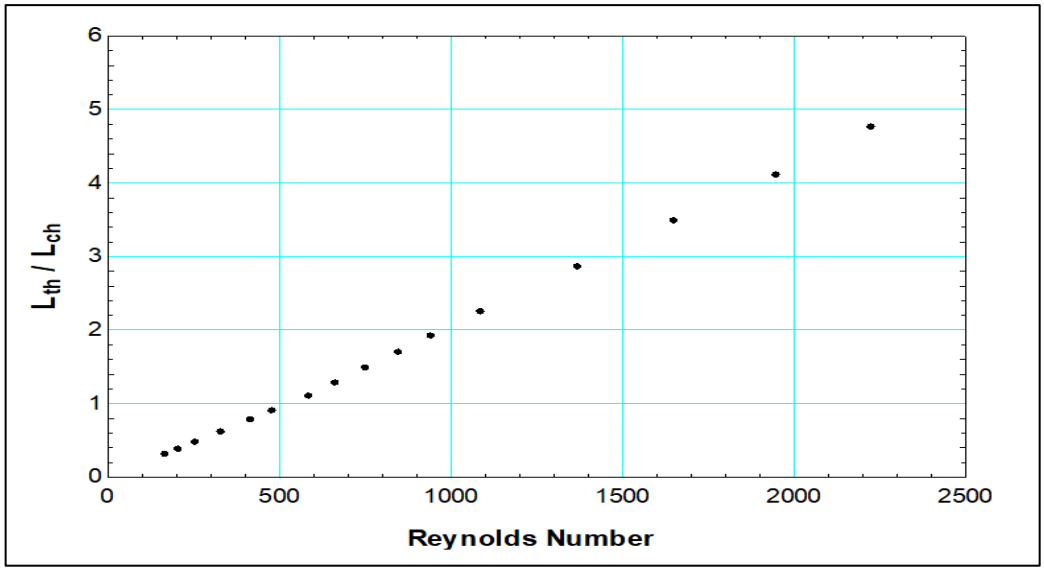

Figure 13: Influence of Reynolds number on the thermal growing length of a micro-channel entry

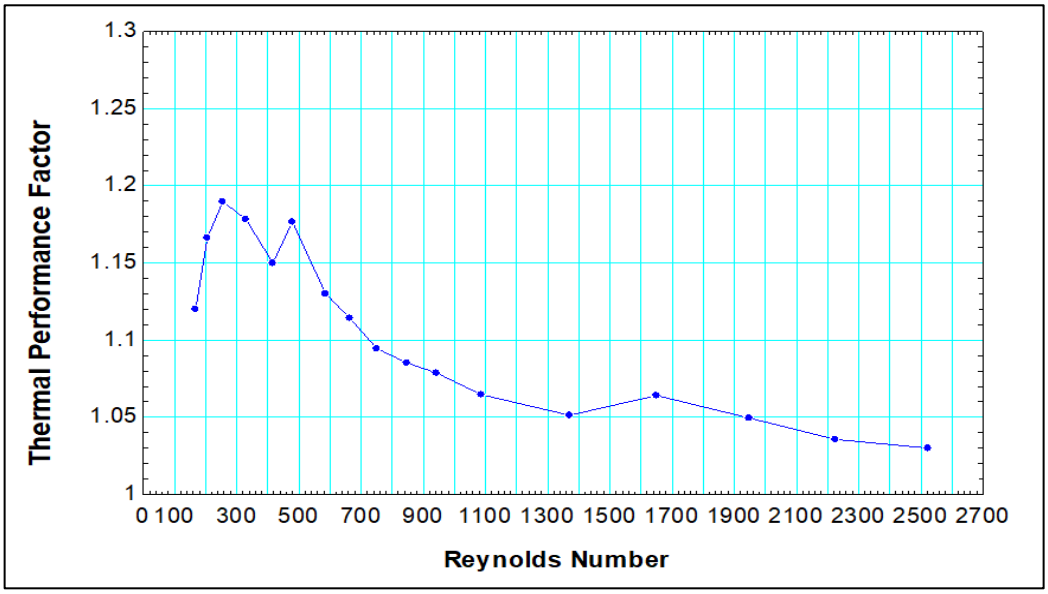

Figure 14: Effect of Reynolds number on thermal performance factor

4. Conclusion

Experimentally, the horizontal single microchannel in single-phase flow was examined. Thus, the tests assess if the experimental data and theoretical predictions differ. Unlike fully developed heat transfer, conventional and coated microchannels have an average Nusselt number that grows with the Reynolds number. As the Reynolds number increases, the Fanning friction factor decreases compared to plain. The results indicate that the coating of Al_2O_3 increases the Fanning friction factor of the microchannel by 3.65% compared to the plain microchannel. Microchannel models with Al_2O_3 coating have a higher average Nusselt number (11.07%) than those with smooth surfaces. A strong thermal performance factor (1.03–1.19) was discovered for the Al_2O_3 coating across all Reynolds numbers. Models coated with Al_2O_3 have higher fanning friction than ordinary microchannels. Traditional correlation effectively estimates the friction factor in conventional microchannels and Al_2O_3coated surfaces. The main contributions of this paper are:

- Investigation by experiment: An experimental examination of single-phase fluid flow and heat transfer in an electroplated microchannel is presented.
- Heat transfer: The microchannel surface electroplating coating increases surface area and fluid flow turbulence, improving heat transmission.

Based on these contributions, further study may include:

- Investigation of alternative coating materials: The study employed electroplating, but other coatings might be examined for heat transmission and pressure drop.
- Study of multi-phase fluid flow: The current work concentrates on single-phase fluid flow; however, coating analysis might give useful insights into system performance.
- Development of modeling and simulation tools: The study showed experimental data, but modeling and simulation tools might forecast coated microchannel performance under varied operating situations. The study focused on the fundamentals of coated microchannels, but they could be applied to experimental methods like microfluidic heat exchangers to evaluate their performance in real-world scenarios.

According to the current findings from experiments, further investigation is required to enhance the designing aspect of the technical field. The major points can be suggested as follows:

1) Investigate the impact of nano coating at inlet and exit manifold geometry on microchannel characteristics.
2) Examine the Effect of various nanocoating methods on microchannel surface characteristics at low mass and high heat flux.
3) Examine the influence of various nanofluid varieties upon the characteristics of flow.

Nomenclature

Symbol	Definition	Units
A	Area	m^2
	Specific heat at constant pressure	J/kg K
D	Diameter	m
f	Fanning friction factor	-

g	Gravitational acceleration	m/s²
G	Mass flux	kg/m² s
h	Heat transfer coefficient	W/m² K
H	Depth	m
(i)	Enthalpy	J/kg
I	Current	A
k	Thermal conductivity	W/m K
L	Length	M
$\dot{m}$	Mass flow rate	kg/s
P	Power	Watt
P	Pressure	Pa
q"	Heat flux	W/m²
Q	Heat	W
(th)	Distance between the thermocouple location and channel base	M
T	Temperature	°C
V	Voltage	V
v	Velocity	m/s
W	Width	M
Z	Distance measured from the inlet channel	M
Re	Reynolds number	
Pr	Prandtl number	
K	thermal conductivity	$W.m^{-1}.K^{-1}$
Nu	local Nusselt number along the heat source	
Greek symbols		
ρ	Density	kg/m³
β	Aspect ratio	-
Δ	Difference, Drop	(K, Pa)
μ	Viscosity	kg/m s
Subscripts		
Symbol	**Description**	
a	Ambient	
app	Apparent	
Avg.	Average	
b	Base	
ch	Channel	
cu	Copper	
Br	Brass	
f	Fluid	
FD	Fully developed flow	
e	Exit	
g	Gas, vapor	
h	Hydraulic	
hy	hydrodynamically developing flow	
I	Inlet	
l	Liquid	
lg	Vaporization	
loss	Loss	
m	Measured	
o	Outlet	
sat	Saturation	
sp	Single-phase	
sc	Sudden contraction	
se	Sudden expansion	

Acknowledgment

This research has been conducted within the Mechanical Engineering Department at the University of Technology. It has been supported by the University of Technology, Ministry of Higher Education and Scientific Research, Baghdad, Iraq, and the self-determined research of authors.

Author contributions

Conceptualization, H. Hussein, E. Fayyadh and M. Hasan; methodology, E. Fayyadh and M. Hasan; validation, H. Hussein; formal analysis, E. Fayyadh and M. Hasan; investigation, H. Hussein; data curation, H. Hussein; writing—review and editing, E. Fayyadh and M. Hasan. All authors have read and agreed to the published version of the manuscript.

Funding

This research received no specific grant from any funding agency in the public, commercial, or not-for-profit sectors.

Data availability statement

The data that support the findings of this study are available on request from the corresponding author.

Conflicts of interest

The authors declare that there is no conflict of interest.

References

[1] I. Mudawar, Recent advances in high-flux, two-phase thermal management, J. Therm. Sci. Eng. Appl., 5 (2013) 1-15. https://doi.org/10.1115/1.4023599

[2] T. M. Harms, M. J. Kazmierczak, and F. M. Gerner, Developing convective heat transfer in deep rectangular microchannels," Int. J. Heat Fluid Flow, 20 (1999) 149–157. https://doi.org/10.1016/S0142-727X(98)10055-3

[3] W. Qu and I. Mudawar, Experimental and numerical study of pressure drop and heat transfer in a single-phase micro-channel heat sink, Int. J. Heat Mass Transf., 45 (2002) 2549–2565. https://doi.org/10.1016/S0017-9310(01)00337-4

[4] P. S. Lee, S. V. Garimella, and D. Liu, Investigation of heat transfer in rectangular microchannels, Int. J. Heat Mass Transf., 48 (2005) 1688–1704. https://doi.org/10.1016/j.ijheatmasstransfer.2004.11.019

[5] J. Y. Jung and H. Y. Kwak, Fluid flow and heat transfer in microchannels with rectangular cross-section, Heat Mass Transf., 44 (2008) 1041–1049. https://doi.org/10.1007/s00231-007-0338-4

[6] N. García-Hernando, A. Acosta-Iborra, U. Ruiz-Rivas, and M. Izquierdo, Experimental investigation of fluid flow and heat transfer in a single-phase liquid flow micro-heat exchanger, Int. J. Heat Mass Transf., 52 (2009) 5433–5446. https://doi.org/10.1016/j.ijheatmasstransfer.2009.06.034

[7] M. Mirmanto, D. B. R. Kenning, J. S. Lewis, and T. G. Karayiannis, Pressure drop and heat transfer characteristics for single-phase developing water flow in rectangular microchannels, J. Phys. Conf. Ser., 395 (2012) 13. https://doi.org/10.1088/1742-6596/395/1/012085

[8] T. Y. Lin and S. G. Kandlikar, An experimental investigation of structured roughness effect on heat transfer during singlephase liquid flow at the microscale, J. Heat Transfer, 134 (2012) 1–9. https://doi.org/10.1115/1.4006844

[9] M. M. Salem, M. H. Elhsnawi, and S. B. Mohamed, Experimental Investigation of Surface Roughness Effect on Single Phase Fluid Flow and Heat Transfer in Micro-Tube, Int. J. Mech. Mechatronics Eng., 7 (2013) 1821–1825. https://doi.org/10.5281/zenodo.1087810

[10] A. Tamayol, J. Yeom, M. Akbari, and M. Bahrami, Low Reynolds number flows across ordered arrays of micro-cylinders embedded in a rectangular micro/minichannel, Int. J. Heat Mass Transf., 58 (2013) 420–426. https://doi.org/10.1016/j.ijheatmasstransfer.2012.10.077

[11] Y. Xing, T. Zhi, L. Haiwang, T. Yitu, Experimental investigation of surface roughness effects on flow behavior and heat transfer characteristics for circular microchannels, Chinese J. Aeronaut., 29 (2016) 1575–1581. https://doi.org/10.1016/j.cja.2016.10.006

[12] B. Markal, O. Aydin, and M. Avci, Experimental study of single-phase fluid flow and heat transfer characteristics in rectangular microchannels, Isi Bilim. Ve Tek. Dergisi/ J. Therm. Sci. Technol., 38 (2018) 65–72.

[13] R. Kumar, M. Islam, and M. M. Hasan, Investigations on Single-Phase Liquid Flow through Semi-Circular Microchannels, Int. J. Appl. Eng. Res., 13 (2018) 6870–6880.

[14] B. Huang, H. Li, S. Xia, and T. Xu, Experimental investigation of the flow and heat transfer performance in micro-channel heat exchangers with cavities, Int. J. Heat Mass Transf., 159 (2020) 1-10. https://doi.org/10.1016/j.ijheatmasstransfer.2020.120075

[15] S. A. Mohammed and E. M. Fayyadh, Effect of artificial cavities on heat transfer and flow characteristics microchannel, Iraqi J. Mech. Mater. Eng., 20 (2020) 180–192 .

[16] T. Alam, W. Li, W. Chang, F. Yang, J. Khan, and C. Li, A comparative study of flow boiling HFE-7100 in silicon nanowire and plain wall microchannels, Int. J. Heat Mass Transf., 124 (2018) 829–840. https://doi.org/10.1016/j.ijheatmasstransfer.2018.04.010

[17] H. Wang, Y. Yang, M. He, and H. Qiu, Subcooled flow boiling heat transfer in a microchannel with chemically patterned surfaces, Int. J. Heat Mass Transf., 140 (2019) 587–597. https://doi.org/10.1016/j.ijheatmasstransfer.2019.06.027

[18] S. K. Gupta and R. D. Misra, Flow boiling heat transfer performance of copper-alumina micro-nanostructured surfaces developed by forced convection electrodeposition technique, Chem. Eng. Process. - Process Intensif., 164 (2021) 108408. https://doi.org/10.1016/j.cep.2021.108408

[19] M. Bulut, M. Shukla, S. G. Kandlikar, & N. Sozbir, Experimental study of heat transfer in a microchannel with pin fins and sintered coatings, Practical Heat Transfer, 36 (2023)1-16. https://doi.org/10.1080/08916152.2023.2176566

[20] M. R. Özdemir, M. M. Mahmoud, and T. G. Karayiannis, Flow Boiling of Water in a Rectangular Metallic Microchannel, Heat Transf. Eng.,42 (2021) 492–516. https://doi.org/10.1080/01457632.2019.1707390

[21] S. G. Kandlikar, S. Garimella, D. Li, S. Colin, and M. R. King, Heat Transfer and Fluid Flow in Minichannels and Microchannels, 2nd Editio. Elsevier, 2014. https://dx.doi.org/10.1016/C2011-0-07521-X

[22] S. A. Mohammed, E. M. Fayyadh, Experimental Investigation of Sub-Cooled Flow Boiling in Metallic Microchannel. Eng. Technol. J., 37 (2019) 408-415. https://doi.org/10.30684/etj.37.10A.5

[23] A. Koşar, C.-J. Kuo, and Y. Peles, Boiling heat transfer in rectangular microchannels with reentrant cavities, Int. J. Heat Mass Transf., 48 (2005) 4867–4886. https://doi.org/10.1016/j.ijheatmasstransfer.2005.06.003

[24] E. M. Fayyadh, M. M. Mahmoud, K. Sefiane, T. G. Karayiannis, Flow boiling heat transfer of R134a in multi microchannels. Int. J. Heat Mass Transf., 110 (2017) 422-436. https://doi.org/10.1016/j.ijheatmasstransfer.2017.03.057

[25] R. K. Shah and A. L. London, Laminar Flow Forced Convection in Ducts. Elsevier, Oxford Academic Press, NY, USA, supplement 1 to advance in heat transfer, J. Fluids Eng., 1978. https://doi.org/10.4236/jamp.2014.27073

[26] R. J. Phillips, Forced-convection, liquid-cooled, microchannel heat sinks, MSc thesis, Massachusetts Institute of Technology, Cambridge, USA, 1987.

[27] Q. A. Al-Nakeeb; E. M. Fayyadh, M. R. Hasan. Experimental Investigation of Artificial Cavities Effect of Single-Phase Fluid Flow and Heat Transfer in Single Microchannel, Eng. Technol. J., 40 (2022) 109-119. https://doi.org/10.30684/etj.v40i1.2122

[28] Shah R.K., and Bhatti M.S. (1987), Laminar Convective Heat Transfer in Ducts" Handbook of Single Phase Convective Heat Transfer, New York:John Wiley.

[29] Blasius H. (1913), "Das aehnlichkeitsgesetz bei reibungsvorgängen in flüssigkeiten", Mitteilungen Über Forschungsarbeiten Auf Dem Gebiete Des Ingenieurwesens, Springer, pp. 1–41.